Silicene-based π and φ_0 Josephson junctions

Xingfei Zhou[1] and Guojun Jin[1,2,*]

[1] *National Laboratory of Solid State Microstructures, Department of Physics, and Collaborative Innovation Center of Advanced Microstructures, Nanjing University, Nanjing 210093, China*

[2] *Department of Physics Science and Technology, Kunming University, Kunming 650214, China*

(Received 5 February 2017; revised manuscript received 8 April 2017; published 18 May 2017)

We investigate the supercurrent in a silicene-based Josephson junction under external-field modulations spatially. Employing the qualitative analysis and solving the Dirac–Bogoliubov–de Gennes equation, it is found that, for the bulk states, a π junction is generated from the valley polarization by combining an antiferromagnetic exchange magnetization and spin-orbit coupling. In contrast, for the topologically protected edge states, a π as well as a φ_0 junction can be obtained by adjusting ferromagnetic exchange field or antiferromagnetic exchange magnetization to shift the edge states in wave vector space; or alternatively by modulating electric and light fields to modify the Fermi velocity of the edge states. It is proposed that a direct current superconducting quantum interference devices can be used to observe these π and φ_0 junctions in experiment.

DOI: 10.1103/PhysRevB.95.195419

I. INTRODUCTION

Recently, the silicene-based superconducting proximity effects, such as Andreev reflection, Andreev bound state (ABS), and 0-π transition, have been studied [1–3]. The process of an electron-hole conversion at the interface between a normal metal and a superconductor is called Andreev reflection [4]. When a Josephson junction is constructed, for a normal metal intermediated between two superconductors, the round-trip Andreev reflection of an electron and a hole will lead to the ABS which supports the supercurrent transport [5]. So far, according to the condition of minimal Josephson free energy, four different types of Josephson junctions are defined, i.e., 0, π, φ, and φ_0 junctions. The $0(\pi)$ junction, which is studied widely [2,6–9], represents the minimum of Josephson free energy at phase difference $\phi = 0(\pi)$. There are two minima of Josephson free energy at $\phi = \pm\varphi$ for a φ junction, which was predicted and observed in a structure consisting of periodic alternating 0 and π junctions [10,11]. By contrast, there is only one minimum of Josephson free energy at $\phi = \varphi_0$ for a φ_0 junction, which was discussed in nanowire-based [12–15] or quantum dot-based [16,17] Josephson junctions applied by the Rashba spin-orbit coupling and the Zeeman field, and a single quantum spin Hall edge applied by a ferromagnetic exchange field [18].

Here we focus our attention on the φ_0 junction in which the current-phase relation can be written as $J = J_c \sin(\phi - \varphi_0)$ with the critical current J_c. Although the φ_0 junction has been studied in several years [12–18], its physical mechanism and experimental realization are still to be explored and developed. In this paper we investigate a silicene-based Josephson junction and clarify three important issues. First, we analyze the difference between bulk and topologically protected edge state-supported Josephson currents. Second, we study the physical mechanism for realization of φ_0 junction by phenomenological theory and numerical calculations, and give the intuitive physical picture for φ_0 junction clearly. Third, we propose a convenient way, by an electric or a light field-manipulated device, to demonstrate the π and φ_0 junctions.

*Corresponding author: gjin@nju.edu.cn

The schematic diagram for a silicene-based Josephson junction is shown in Fig. 1. The superconducting regions are realized by the superconducting proximity effect. The normal region could be applied by a perpendicular electric field, an off-resonant light, an antiferromagnetic exchange magnetization, and a ferromagnetic exchange field [19]. Generally speaking, both the bulk and edge states can exist in a silicene nanoribbon by adjusting the Fermi energy. For the purpose of comparison, we first discuss the Josephson effect in the bulk states, which shows a π junction in the presence of an antiferromagnetic exchange magnetization. Reminding that the pristine silicene is a quantum spin Hall insulator with two helical edges [20], we then make a deep investigation on the Josephson effect in the edge states. It has been known that when a ferromagnetic exchange field is applied in a single edge, a φ_0 junction is generated [18]. Unfortunately, when the ferromagnetic exchange field is applied in both edges, the effect showing a φ_0 junction reduces and even disappears. Gratifyingly, when an antiferromagnetic exchange magnetization is applied in a single or two edges, the φ_0 junction always exists. Especially, there is another mechanism, using a light field to modify the Fermi velocity of the edge states, for realizing the π and φ_0 junctions.

This paper is organized as follows. In Sec. II the model and basic formulas are constructed. In Secs. III and IV the theoretical treatments and numerical results for the bulk and edge states-supported Josephson currents are presented and discussed, respectively. In Sec. V a direct current superconducting quantum interference devices (dc SQUID) is proposed to observe the π and φ_0 junctions. Finally, in Sec. VI the conclusion of this work is given.

II. MODEL AND FORMALISM

Based on the second-nearest-neighbor tight-binding model, the Hamiltonian of silicene is [20–22]

$$\begin{aligned}\mathcal{H} = &-t \sum_{\langle i,j\rangle\alpha} c_{i\alpha}^\dagger c_{j\alpha} + i\frac{\lambda_{\mathrm{so}}}{3\sqrt{3}} \sum_{\langle\langle i,j\rangle\rangle\alpha\beta} \nu_{ij} c_{i\alpha}^\dagger \sigma_{\alpha\beta}^z c_{j\beta} \\ &- lE_z \sum_{i\alpha} \mu_i c_{i\alpha}^\dagger c_{i\alpha} + i\frac{\lambda_\omega}{3\sqrt{3}} \sum_{\langle\langle i,j\rangle\rangle\alpha\beta} \nu_{ij} c_{i\alpha}^\dagger c_{j\beta} \\ &- \lambda_{\mathrm{F}} \sum_{i\alpha} c_{i\alpha}^\dagger \sigma_{\alpha\alpha}^z c_{i\alpha} + \lambda_{\mathrm{AF}} \sum_{i\alpha} \mu_i c_{i\alpha}^\dagger \sigma_{\alpha\alpha}^z c_{i\alpha}, \qquad (1)\end{aligned}$$

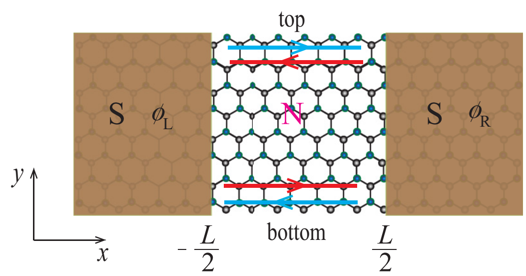

FIG. 1. Schematic diagram for the top view of a silicene-based Josephson junction. A zigzag silicene nanoribbon is considered. The red (blue) line represents down (up) spin. A perpendicular electric field, an off-resonant light, a ferromagnetic exchange field, and an antiferromagnetic exchange magnetization can be applied in the normal (N) region. The left and right regions are superconducting (S) regions which are realized by applying the s-wave superconductors in silicene.

where $c^{\dagger}_{i\alpha(\beta)}$ ($c_{i\alpha(\beta)}$) is the creation (annihilation) operator of an electron with spin index $\alpha(\beta)$ at site i. $\langle i,j\rangle$ ($\langle\langle i,j\rangle\rangle$) denotes that electrons run over all the nearest-neighbor (next-nearest-neighbor) hopping sites. The first term of the Hamiltonian is the nearest-neighbor hopping with the hopping integral $t = 1.6$ eV. The second term is the spin-orbit coupling with $\lambda_{\mathrm{so}} = 3.9$ meV, where $\sigma^z_{\alpha\beta}$ is the Pauli matrix of spin and $\nu_{ij} = 1\,(-1)$ if the next-neighboring hopping is anticlockwise (clockwise) with respect to the positive z axis. The third term is a stagger potential modulated by the perpendicular electric field E_z for the buckled structure, i.e., the two sublattice planes are separated by a distance $2l$ with $l = 0.23$ Å. The fourth term is the off-resonant right-circularly polarized light with illumination parameter λ_ω [21,23,24]. We should point out that the modulation of time-dependent off-resonant light is transformed into an static modulation based on the Floquet theory [25]. The last two terms are the ferromagnetic exchange field and the antiferromagnetic exchange magnetization [26] with the exchange constants λ_{F} and λ_{AF}, respectively.

For revealing the property of bulk states simply and clearly, in the low-energy approximation, the effective Hamiltonian near K (K') valley can be written in the wave vector space as

$$\mathcal{H}_\eta = \hbar v_{\mathrm{F}}(k_x\tau_x + \eta k_y\tau_y) + \eta\lambda_{\mathrm{so}}\sigma_z\tau_z - lE_z\tau_z + \eta\lambda_\omega\tau_z - \lambda_{\mathrm{F}}\sigma_z + \lambda_{\mathrm{AF}}\sigma_z\tau_z, \tag{2}$$

where $\eta = \pm$ denote the two valleys of the band structure, $v_{\mathrm{F}} = 5.5\times10^5$ m/s is the Fermi velocity, and $\tau_{x,y,z}$ and σ_z are the 2×2 Pauli matrices of the sublattice pseudospin and real spin. According to the tight-binding model, the energy bands of zigzag silicene nanoribbon with different external-field parameters lE_z, λ_ω, λ_{F}, and λ_{AF} are plotted in Fig. 2.

The Hamiltonian of the edges in the zigzag nanoribbon can be written as [27]

$$\mathcal{H}_{\mathrm{edge}} = s_z\left(\frac{\sigma_z\lambda_{\mathrm{so}} + \lambda_\omega}{t}\hbar v_{\mathrm{F}}k_x - s_z\sigma_z\lambda_{\mathrm{F}} + \sigma_z\lambda_{\mathrm{AF}} + lE_z\right), \tag{3}$$

where σ_z and s_z being the Pauli matrices represent spin and edge index, respectively. From Fig. 2 and Eq. (3) it is obvious

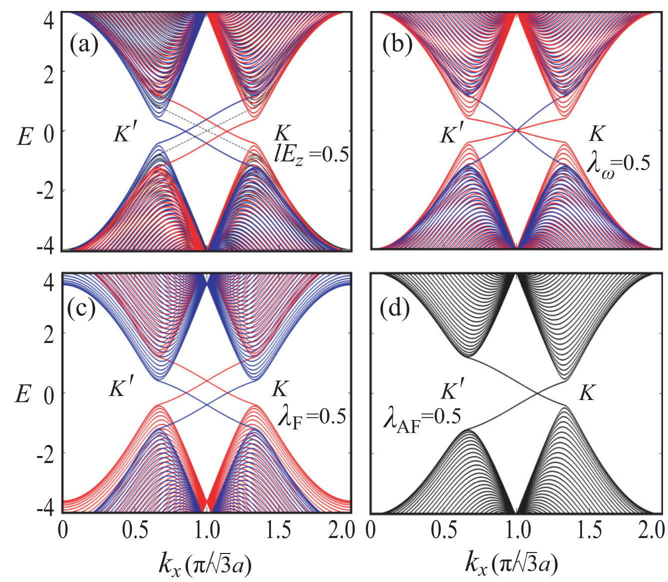

FIG. 2. Dispersion relations of a zigzag silicene nanoribbon in different external fields, separately. (a) In the pristine state (the black dashed line) and in the perpendicular electric field with parameter lE_z (the blue and red lines); (b) in the off-resonant light with illumination parameter λ_ω; (c) in the ferromagnetic exchange field with parameter λ_{F}; and (d) in the antiferromagnetic exchange magnetization with parameter λ_{AF}, respectively. The black line is the superposition of blue (up spin) and red (down spin) lines. The unit for energy is λ_{so} and the width of nanoribbon $W = 128$ atoms.

that the external parameters, including lE_z, λ_{F}, and λ_{AF}, induce the translation of the dispersion of edge states in the wave vector space while the Fermi velocity of the edge states is modulated by the off-resonant light λ_ω, which will bring significant results shown in Sec. IV. We need to notice that λ_{F}, λ_{AF}, lE_z, and λ_ω should all be smaller than the spin-orbit coupling λ_{so}, otherwise the edge states will disappear as was discussed in Ref. [22] in detail. In the calculations, we keep the edge states in the quantum spin Hall regime.

Generally [1,2], the Dirac–Bogoliubov–de Gennes (DBdG) equation for the bulk states is

$$\begin{pmatrix} \mathcal{H}_{\eta\sigma} - m_{\eta\sigma} - E_{\mathrm{F}} & \Delta(T) \\ \Delta^*(T) & E_{\mathrm{F}} - (\mathcal{H}_{\eta\sigma} + m_{\eta\sigma}) \end{pmatrix}\begin{pmatrix} u_e \\ v_h \end{pmatrix} = \varepsilon\begin{pmatrix} u_e \\ v_h \end{pmatrix}, \tag{4}$$

where $\mathcal{H}_{\eta\sigma} = \hbar v_{\mathrm{F}}(k_x\tau_x + \eta k_y\tau_y) + \eta\sigma\lambda_{\mathrm{so}}\tau_z - lE_z\tau_z - U\hat{\mathrm{I}}$ and $m_{\eta\sigma} = \sigma\lambda_{\mathrm{F}}\hat{\mathrm{I}} - (\eta\lambda_\omega + \sigma\lambda_{\mathrm{AF}})\tau_z$. Here σ is the spin index, $\hat{\mathrm{I}}$ is the unit matrix, and $U = U_0[\Theta(x - L/2) + \Theta(-L/2 - x)]$ with the Heaviside step function $\Theta(x)$ and the positive electrostatic potential U_0. ε is the excited energy relative to the Fermi level E_{F} and u_e (v_h) is the electronlike (holelike) quasiparticle wave function. $\Delta(T) = 0$ in the normal region, while $\Delta(T) = \Delta_0 \tanh(1.74\sqrt{\frac{T_c}{T} - 1})e^{i\phi_{\mathrm{L(R)}}}$ with Δ_0 the zero-temperature energy gap, T_c the transition temperature, and $\phi_{\mathrm{L(R)}}$ the macroscopic phase in the left and right superconducting regions. In the calculations we adopt $k_{\mathrm{B}}T_c = \frac{2\Delta_0}{3.53}$ with $\Delta_0 = 1$ meV which is used as the energy unit. It is well known that the ABS plays a key role for calculating the supercurrent. In the equilibrium regime, by summing over the positive ABS energy $\varepsilon_{n\eta\sigma}$ of subgap quasiparticles at finite temperature T, the Josephson current J passing through the junction is given as

$$J = -\frac{2e}{\hbar}\sum_{n\eta\sigma}\int N(\varepsilon_{n\eta\sigma})\tanh\left(\frac{\varepsilon_{n\eta\sigma}}{2k_{\mathrm{B}}T}\right)\frac{d\varepsilon_{n\eta\sigma}}{d\phi}\cos\theta d\theta, \quad (5)$$

where n represents the number of ABSs, $N(\varepsilon_{n\eta\sigma}) = (W/\pi\hbar v_{\mathrm{F}})\sqrt{(\varepsilon_{n\eta\sigma}+E_{\mathrm{F}}+\sigma\lambda_{\mathrm{F}})^2 - M_{\eta\sigma}^2}$ with $M_{\eta\sigma} = \eta\sigma\lambda_{\mathrm{so}} - lE_z + \eta\lambda_\omega + \sigma\lambda_{\mathrm{AF}}$ is the number of the transverse mode in a silicene monolayer of width W, θ is the incident angle, and $\phi = \phi_{\mathrm{R}} - \phi_{\mathrm{L}}$ is the phase difference.

After some algebraic operations and matrix transformations, the simplified DBdG equation for the edge states is

$$\begin{pmatrix} -i\hbar v_{\mathrm{F}}^s\partial_x + A & \Delta(T) \\ \Delta^*(T) & i\hbar\bar{v}_{\mathrm{F}}^s\partial_x + B\end{pmatrix}\begin{pmatrix} u_e \\ v_h\end{pmatrix} = \varepsilon\begin{pmatrix} u_e \\ v_h\end{pmatrix}, \quad (6)$$

with

$$\begin{aligned} A &= -s\lambda_{\mathrm{F}} + slE_z + \lambda_{\mathrm{AF}} - E_{\mathrm{F}}, \\ B &= E_{\mathrm{F}} - (s\lambda_{\mathrm{F}} + slE_z - \lambda_{\mathrm{AF}}). \end{aligned} \quad (7)$$

Here $s = \pm 1$ represent the top and bottom edge states, $v_{\mathrm{F}}^s(\bar{v}_{\mathrm{F}}^s) = \frac{\lambda_{\mathrm{so}}+(-)s\lambda_\omega}{t}v_{\mathrm{F}}$ is the velocity of electron (hole) in the normal region, and $v_{\mathrm{F}}^s = \bar{v}_{\mathrm{F}}^s = v_{\mathrm{F}}' = \frac{\lambda_{\mathrm{so}}}{t}v_{\mathrm{F}}$ in the superconducting regions. We define that, in the normal region, the first (second) line in Eq. (6) represents the electron (hole) moving toward the right (left), or vice verse. Besides, spin is dependent on the direction of moving particles due to the helicity of the edge states.

The wave functions of electron and hole in the normal region and the wave functions of quasiparticle in the superconducting regions are given by solving Eq. (6), respectively. They are

$$\begin{aligned} \psi_e &= \begin{pmatrix} 1 \\ 0\end{pmatrix}e^{ik_e x}, \quad \psi_h = \begin{pmatrix} 0 \\ 1\end{pmatrix}e^{-ik_h x}, \\ \psi_{\mathrm{SL(R)}}^{\pm} &= \begin{pmatrix} e^{\pm i\beta} \\ e^{-i\phi_{\mathrm{L(R)}}}\end{pmatrix}e^{ik^{\pm}x}, \end{aligned} \quad (8)$$

where

$$\beta = \begin{cases} -i\,\mathrm{arcosh}[\varepsilon/\Delta(T)], & \varepsilon > \Delta(T), \\ \arccos[\varepsilon/\Delta(T)], & \varepsilon < \Delta(T), \end{cases} \quad (9)$$

and k_e, k_h, and $k^{\pm}$ are the wave vectors of electron, hole, and quasiparticle, respectively, which are defined as

$$k_e = \frac{\varepsilon - A}{\hbar v_{\mathrm{F}}^s}, \quad k_h = \frac{\varepsilon - B}{\hbar\bar{v}_{\mathrm{F}}^s}, \quad k^{\pm} = \frac{E_{\mathrm{F}} \pm \sqrt{\varepsilon^2 - \Delta^2}}{\hbar v_{\mathrm{F}}'}. \quad (10)$$

According to the continuity of wave function, we match the states at the interfaces ($x = \pm L/2$) between S and N regions, i.e.,

$$\begin{aligned} a\psi_{\mathrm{SL}}^{-}(-L/2) &= c\psi_e(-L/2) + d\psi_h(-L/2), \\ b\psi_{\mathrm{SR}}^{+}(L/2) &= c\psi_e(L/2) + d\psi_h(L/2). \end{aligned} \quad (11)$$

In the short-junction regime, the levels for the ABSs are obtained as

$$\varepsilon = \pm\Delta(T)\cos\left[\frac{\phi}{2} - (k_e + k_h)\frac{L}{2}\right]. \quad (12)$$

By summing over the ABS levels at finite temperature T, the Josephson current J passing through the junction is given as

$$J = -\frac{2e}{\hbar}\sum_s \tanh\left(\frac{|\varepsilon|}{2k_{\mathrm{B}}T}\right)\frac{d|\varepsilon|}{d\phi}. \quad (13)$$

It should be pointed out that, although the ABS levels have a 4π periodicity, the Josephson current still remains with a 2π periodicity in the equilibrium regime. If the nonequilibrium regime is considered [28–30], the Josephson current will show a 4π periodicity due to the Majorana bound states.

III. BULK STATES

In order to show the properties of Josephson current contributed from the bulk states distinctly, we deal with the low-energy effective Hamiltonian in Eq. (2) and the related DBdG equation in Eq. (4). It is noted that the Josephson effect modulated by ferromagnetic exchange field and off-resonant light was investigated and a π junction was predicted [2,3]. So here we mainly study the Josephson effect modulated by antiferromagnetic exchange magnetization.

Before presenting the numerical results, we give a qualitative analysis first. It has been argued that, in silicene, a Cooper pair is composed of one electron with up (down) spin in K valley and the other electron with down (up) spin in K' valley [1]. From Eq. (2), the dispersion relation in the normal region is obtained as

$$E_{\eta\sigma} = \pm\sqrt{(\hbar v_{\mathrm{F}}k)^2 + (\eta\sigma\lambda_{\mathrm{so}} - lE_z + \sigma\lambda_{\mathrm{AF}})^2}. \quad (14)$$

Considering the normal incidence, two paired electrons at the Fermi energy [31] will have the center-of-mass wave vector

$$2q = k_x(\eta,\sigma) - k_x(-\eta,-\sigma), \quad (15)$$

where $k_x(\eta,\sigma) = \sqrt{E_{\mathrm{F}}^2 - (\eta\sigma\lambda_{\mathrm{so}} - lE_z + \sigma\lambda_{\mathrm{AF}})^2}/\hbar v_{\mathrm{F}}$ derived from Eq. (14). It is a key point that the nonzero q appears if $\lambda_{\mathrm{AF}} \neq 0$, which will lead to the Josephson current reversal. When the electric field is neglected, then $k_x(\eta,\sigma) = \sqrt{E_{\mathrm{F}}^2 - (\eta\lambda_{\mathrm{so}} + \lambda_{\mathrm{AF}})^2}/\hbar v_{\mathrm{F}}$. It is clear that the valley polarization plays an important role in the realization of π junction. The detailed pairing cases for nonzero λ_{AF} are shown in Fig. 3.

In the superconducting regions, there is a zero center-of-mass wave vector for Cooper pairs in the ground state and then a phenomenological macroscopic wave function can be taken as $\Psi(x) = \Psi_0 e^{i\phi_s}$ with Ψ_0 being the amplitude of the order parameter and ϕ_s the macroscopic phase. When a Cooper pair in a superconducting region penetrates into the normal region, at first, the phenomenological macroscopic wave function is changed into $\Psi(x) = \Psi_0 e^{-\frac{x}{\xi}}e^{i\phi_s}$ with ξ the superconducting coherence. However, as shown in Fig. 3, in the presence of λ_{AF}, the normal region is valley polarized and then two electrons from opposite valleys near the Fermi surface with opposite spins constitute a Cooper pair with a nonzero

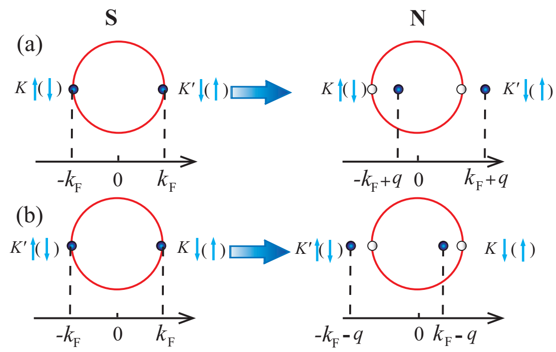

FIG. 3. (a) and (b) In the presence of λ_{AF}, four possible pairing cases of two electrons are shown in the superconducting and normal regions, respectively. Here the red circles represent the Fermi surface. S (N) denotes the superconducting (normal) region.

center-of-mass wave vector $2q = [\sqrt{E_{\mathrm{F}}^2 - (-\lambda_{\mathrm{so}} + \lambda_{\mathrm{AF}})^2} - \sqrt{E_{\mathrm{F}}^2 - (\lambda_{\mathrm{so}} + \lambda_{\mathrm{AF}})^2}]/\hbar v_{\mathrm{F}}$. Correspondingly, the additional phase factor $e^{\pm i2qx}$ is obtained through the normal region. It is obvious that the valley polarization, similar to the spin polarization arisen from a ferromagnetic exchange field [31], can also lead to the nonzero center-of-mass wave vector. This is an interesting result, which is unique in silicene and cannot appear in graphene due to the very weak spin-orbit coupling for the latter.

Therefore, the phenomenological macroscopic wave function will be modulated by the nonzero center-of-mass wave vector in the normal region from Fig. 3 [31,32], that is

$$\begin{aligned}\Psi(x) &= \Psi_{K\uparrow K'\downarrow} + \Psi_{K'\uparrow K\downarrow} + \Psi_{K\downarrow K'\uparrow} + \Psi_{K'\downarrow K\uparrow}\\ &= \Psi_0 e^{-\frac{x}{\xi}} e^{i\phi_s}(e^{-i2qx} + e^{i2qx} + e^{-i2qx} + e^{i2qx})\\ &= 4\Psi_0 \cos(2qx) e^{-\frac{x}{\xi}} e^{i\phi_s}. \end{aligned} \tag{16}$$

This superposed state in Eq. (16) is like the Fulde-Ferrel-Larkin-Ovchinnikov state [33,34] in which the pair wave function oscillates periodically in space. Using the chosen coordinate in Fig. 1, we can give the macroscopic wave function, as a superposition state of the macroscopic wave functions from both left and right superconductors, in the normal region,

$$\begin{aligned}\Psi(x) = 4\Psi_0\{&\cos[2q(x+L/2)]e^{-\frac{x+L/2}{\xi}} e^{-i\frac{\phi}{2}}\\ &+ \cos[2q(x-L/2)]e^{\frac{x-L/2}{\xi}} e^{i\frac{\phi}{2}}\}.\end{aligned} \tag{17}$$

Here we choose $\phi_{\mathrm{L}} = -\phi/2$ and $\phi_{\mathrm{R}} = \phi/2$.

According to the Ginzburg-Landau equation [35], the supercurrent $J \sim -i(\Psi^*\nabla\Psi - \Psi\nabla\Psi^*)$, and taking $x = L/2$, we obtain the following phenomenological Josephson current:

$$J \sim 4\sin\phi\left[q\sin(2qL) + \frac{1}{\xi}\cos(2qL)\right]e^{-\frac{L}{\xi}}, \tag{18}$$

which is similar to the result from the superconductor-ferromagnet-superconductor Josephson junction [36]. From the perspective of this qualitative analysis, the valley polarization arising from the interaction between λ_{so} and λ_{AF} can generate a π junction. Our phenomenological assessment will be confirmed by the numerical calculations in the next paragraph.

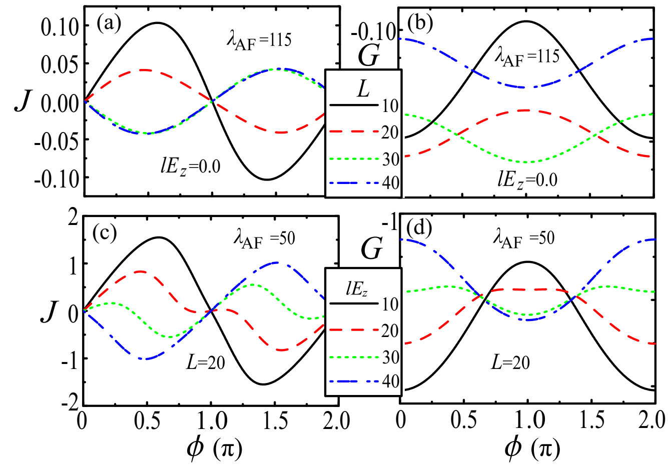

FIG. 4. (a)–(d) Josephson current and free energy versus the phase difference are shown in different λ_{AF}, L, and lE_z, respectively. The units for junction length and free energy are 1 nm and $\frac{WE_{\mathrm{F}}}{\pi\hbar v_{\mathrm{F}}}\Delta_0$, respectively.

We analyze the Josephson effect in the experimentally most relevant short-junction regime that the length L of the normal region is smaller than the superconducting coherence length ξ, i.e., $L \ll \frac{\hbar v_{\mathrm{F}}}{\Delta_0} \approx 362$ nm. Then we can obtain the similar formalism of the ABS shown in Ref. [2] by the method that the illumination parameter ηF_ω is replaced by the parameter $\sigma\lambda_{\mathrm{AF}}$. In terms of Eq. (5), we have calculated the ϕ-dependent Josephson current and free energy with different parameters lE_z, λ_{AF}, and junction length L at $k_{\mathrm{B}}T = 0.1\Delta_0$, as shown in Fig. 4. The unit for Josephson current is $J_0 = \frac{2e}{\hbar}\frac{WE_{\mathrm{F}}}{\pi\hbar v_{\mathrm{F}}}$ and the Fermi energy is chosen at $E_{\mathrm{F}} = 120$ meV. In the presence of λ_{AF}, the 0-π transition appears, clearly shown in Fig. 4(a). The 0 and π state can be verified by calculating the free energy [37]

$$G = -k_{\mathrm{B}}T\sum_{n\eta\sigma}\int N(\varepsilon_{n\eta\sigma})\ln\left[2\cosh\left(\frac{\varepsilon_{n\eta\sigma}}{2k_{\mathrm{B}}T}\right)\right]\cos\theta d\theta, \tag{19}$$

shown in Fig. 4(b). These numerical results are consistent with the preceding qualitative analysis. Although it is not convenient to realize the 0-π transition by changing the junction length, the control of perpendicular electric field is feasible in experiment. In Figs. 4(c) and 4(d) there is obviously the electric field-modulated 0-π transition. It deserves to stress that the π junction here generated by the interaction between the antiferromagnetic exchange magnetization and spin-orbit coupling is different from the one generated by the interaction between the off-resonant light and spin-orbit coupling in Ref. [2]. The former arises from the valley polarization while the latter comes from the spin polarization.

IV. EDGE STATES

From edge states, we will give two different types of mechanism for realizing the π and φ_0 junctions. In Sec. IV A the shift of edge states in wave vector space, arising from the exchange constants λ_{F} or λ_{AF}, is viewed as a key role for realizing the π and φ_0 junctions. However, in Sec. IV B the modified Fermi

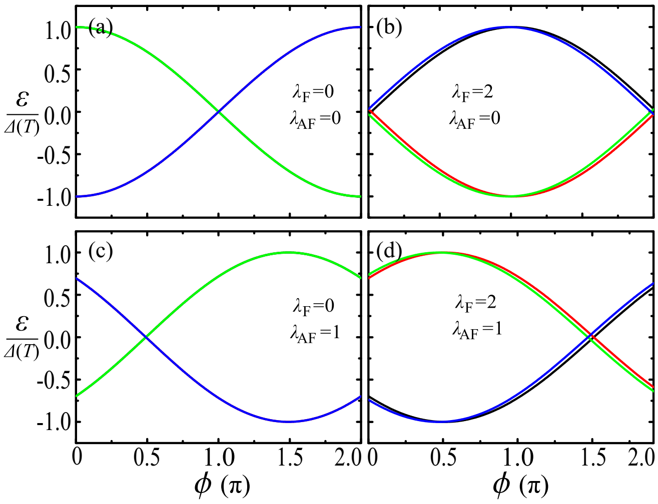

FIG. 5. (a)–(d) Andreev bound state level versus the phase difference with different λ_F and λ_{AF}. The black and red lines belong to the top edge while the green and purple lines belong to the bottom edge. E_z is an arbitrary value below the critical electric field, E_F is placed in the gap, and the junction length L is 20 nm.

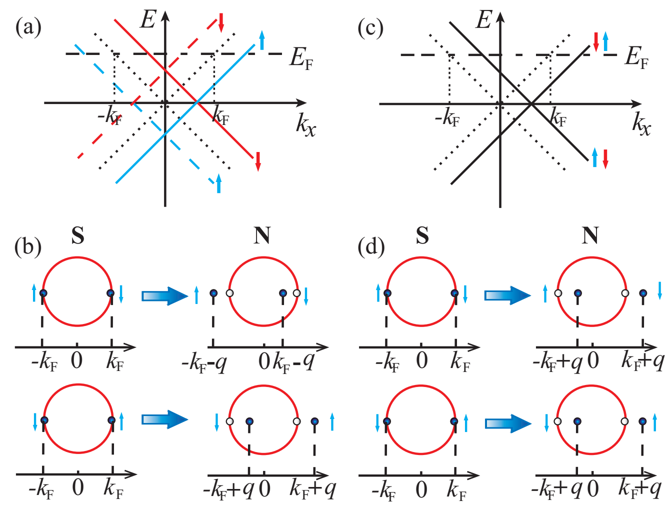

FIG. 6. (a) Schematic diagram for the dispersion relations of the two edge states with the exchange field λ_F. The black dotted lines are the pristine dispersion relation. The red and blue solid (dashed) lines belong to the top (bottom) edge. (b) The possible pairing cases of two electrons are shown in the superconducting and normal regions, respectively. (c) and (d) The corresponding dispersion relations and possible pairing cases in the presence of λ_{AF}. The black solid lines denote the dispersion relations of the edge states with spin degeneracy. Here the red circles in (b) and (d) represent the Fermi surface.

velocity of edge states, coming from the interaction between the spin-orbit coupling λ_{so} and illumination parameter λ_ω, plays a vital role in the realization of the π and φ_0 junctions.

A. Shift of edge states in wave vector space

If we neglect the off-resonant light, then Eq. (12) is written as

$$\varepsilon = \pm\Delta(T)\cos\left(\frac{\phi}{2} - \frac{s\lambda_F - \lambda_{AF}}{\hbar v_F'}L\right). \tag{20}$$

From the equation above, the levels of phase-dependent ABSs in each edge are plotted with different parameters λ_F and λ_{AF} in Fig. 5. In order to keep the topological edge states, the values of lE_z, λ_F, and λ_{AF} should be smaller than λ_{so}. The ABS levels in Fig. 5(a) reproduce the results in Ref. [29] and are not affected by E_z due to the time-reversal symmetry. When λ_F is applied, the ABS levels in the bottom and top edges are not symmetric about the point $\phi = \pi$, but the shapes of entire ABS levels are symmetric about $\phi = \pi$, shown in Fig. 5(b). It is easy to find that ABS levels $\varepsilon = \pm\Delta(T)\cos(\frac{\phi}{2} - \frac{s\lambda_F}{\hbar v_F'}L)$ with the ferromagnetic exchange field in each edge. Then the sum of ABS levels in each edge gives $\varepsilon = \pm\Delta(T)\cos(\frac{\lambda_F}{\hbar v_F'}L)\cos(\frac{\phi}{2})$. These are similar to the ABSs of the π junction when $\cos(\frac{\lambda_F}{\hbar v_F'}L) < 0$ [2]. When a ferromagnetic exchange field is applied in an single edge, the ABSs are the same as the ones in Ref. [18], showing a φ_0 junction in which an anomalous Josephson current, i.e., a finite Josephson current at the zero phase difference, is generated. However, if λ_F is applied in both edges, the other edge will suppress this φ_0 junction effect. But this suppression will become a cooperative effect when an antiferromagnetic exchange magnetization is applied in the normal region, shown in Fig. 5(c). This result can be obtained from Eq. (20) easily. Interestingly, as shown in Fig. 5(d), when λ_F and λ_{AF} are applied in the normal region simultaneously, the superposition of ABS levels in two edges gives $\varepsilon = \pm\Delta(T)\cos(\frac{\lambda_F}{\hbar v_F'}L)\cos(\frac{\phi}{2} + \frac{\lambda_{AF}}{\hbar v_F'}L)$. If $\cos(\frac{\lambda_F}{\hbar v_F'}L) < 0$, the anomalous Josephson current will be reversed. All the speculations from the ABSs will be verified in Figs. 6 and 7.

Similar to the case for the bulk states, before giving the numerical results for Josephson current, we first make a qualitative analysis by using the phenomenological theory. According to the dispersion relation in Fig. 2 and Eq. (3), all the possible pairing cases are shown in the superconducting and normal regions in Fig. 6, respectively. In the normal region applied by a ferromagnetic exchange field, shown in Figs. 6(a) and 6(b), two electrons with opposite spins near the Fermi surface constitute a Cooper pair with a nonzero center-of-mass wave vector $2q = 2\lambda_F/\hbar v_F'$. Following the same method introduced in Sec. III, the phenomenological macroscopic

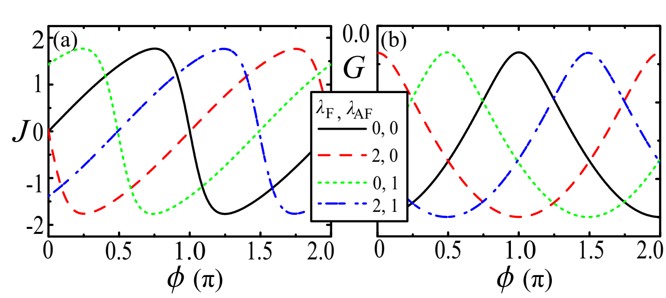

FIG. 7. (a) and (b) Josephson current and free energy versus the phase difference are shown for the different parameters of λ_F and λ_{AF}, respectively. The junction length L is 20 nm. The units for J and G are $e\Delta_0/\hbar$ and Δ_0, respectively.

wave function modulated by the nonzero center-of-mass wave vector is

$$\begin{aligned}\Psi(x) &= \Psi_{\uparrow\downarrow} + \Psi_{\downarrow\uparrow} \\ &= \Psi_0 e^{-\frac{x}{\xi}} e^{i\phi_s}(e^{i2qx} + e^{-i2qx}) \\ &= 2\Psi_0 \cos(2qx) e^{-\frac{x}{\xi}} e^{i\phi_s}. \end{aligned} \tag{21}$$

From the wave function above, we can obtain the same Josephson current shown in Eq. (18). It is easy to find that there is $q = 0$ in the absence of λ_{F}, which leads to the normal Josephson current $J \sim \sin\phi$. From these simple analysis and discussion, we can draw a general conclusion that the ferromagnetic exchange field applied in both edges can induce a π junction. Likely, when λ_{AF} is applied in the normal region, shown in Figs. 6(c) and 6(d), we have the nonzero center-of-mass wave vector $2q = 2\lambda_{\mathrm{AF}}/\hbar v'_{\mathrm{F}}$ and the phenomenological macroscopic wave function is

$$\begin{aligned}\Psi(x) &= \Psi_{\uparrow\downarrow} + \Psi_{\downarrow\uparrow} \\ &= \Psi_0 e^{-\frac{x}{\xi}} e^{i\phi_s}(e^{-i2qx} + e^{-i2qx}) \\ &= 2\Psi_0 e^{-i2qx} e^{-\frac{x}{\xi}} e^{i\phi_s}. \end{aligned} \tag{22}$$

Following the same process of calculations in the case of λ_{F}, we obtain the phenomenological Josephson current in the short-junction regime

$$J \sim 4\sin(\phi + 2qL)e^{-\frac{L}{\xi}}. \tag{23}$$

It is obvious that a φ_0 junction is generated. These qualitative results will be confirmed by the numerical calculations given below.

From Eqs. (13) and (20), the phase-dependent Josephson current is calculated with different λ_{F} and λ_{AF} in Fig. 7(a). The π and φ_0 junctions are shown clearly, which is consistent with the qualitative analysis. We need to notice that $L \ll \frac{\hbar v'_{\mathrm{F}}}{\Delta_0} \approx 0.878$ nm if $\Delta_0 = 1$ meV in the short-junction regime. This seems difficult in experiment. Fortunately, $L \ll 87.8$ nm if $\Delta_0 = 0.01$ meV or $L \ll 101.1(274.4)$ nm if $\Delta_0 = 0.1$ meV and $\lambda_{\mathrm{so}} = 43(100)$ meV in germanene (stanene) [24]. In order to show π and φ_0 junctions clearly, the phase-dependent free energy [37]

$$G = -k_{\mathrm{B}}T \sum \ln\left[2\cosh\left(\frac{|\varepsilon|}{2k_{\mathrm{B}}T}\right)\right] \tag{24}$$

is plotted with different λ_{F} and λ_{AF} in Fig. 7(b). In the presence or absence of E_z, the Josephson junction is always the 0 junction due to the time-reversal symmetry. It becomes a π junction when λ_{F} is applied in both edges. This can be speculated by the critical current $J_c \sim \cos(\frac{\lambda_{\mathrm{F}}}{\hbar v'_{\mathrm{F}}}L) = -0.031 < 0$ derived from Eqs. (13) and (20). When the antiferromagnetic exchange magnetization is applied, a φ_0 junction is generated and $\varphi_0 = -\frac{2\lambda_{\mathrm{AF}}L}{\hbar v'_{\mathrm{F}}} = 4.66 - 16\pi$ derived from Eq. (20). Similarly, in the presence of λ_{F} and λ_{AF}, $\varphi_0 = \pi - \frac{2\lambda_{\mathrm{AF}}L}{\hbar v'_{\mathrm{F}}} = 1.52 - 14\pi$. As the multiples of 2π make no difference, these analytical results are well consistent with the numerical ones ($\varphi_0 = 4.74$ and 1.6) in Fig. 7(b).

The above analysis and numerical calculations, in Figs. 6 and 7, are considered in the case that the external fields are applied in both edges. In fact, we can change the position of

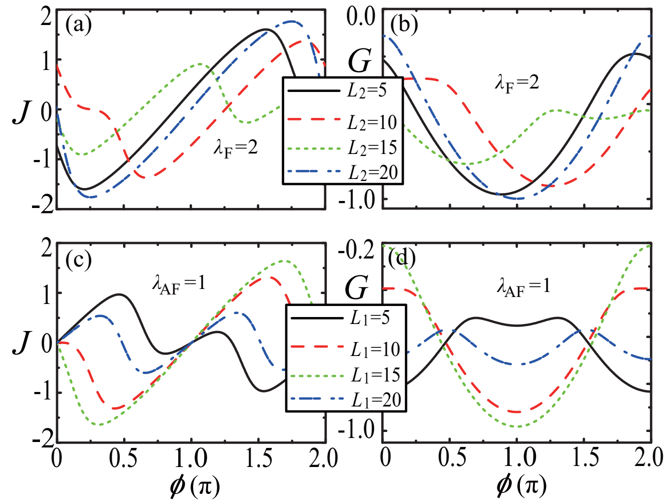

FIG. 8. In the presence of λ_{F} (λ_{AF}), Josephson current and free energy versus the phase difference are shown in (a) and (b) [(c) and (d)] with different junction lengths, respectively. Here $L_1 = 20$ in (a) and (b) while $\frac{\lambda_{\mathrm{AF}}}{\hbar v'_{\mathrm{F}}}(L_1 + L_2) = 8\pi$ in (c) and (d). The units for J and G are the same as the ones in Fig. 7.

external fields and even the junction length artificially. It has been discussed that the ferromagnetic exchange field applied in a single edge could lead to a φ_0 junction [18], while in two edges we can here get a π junction. From Eq. (20), the Cooper pairs through the top (bottom) edge will acquire an additional phase $+(-)\frac{2\lambda_{\mathrm{F}}L}{\hbar v'_{\mathrm{F}}}$. The two opposite phases offset each other and lead to the disappearance of φ_0 junction. But, if the junction lengths of the bottom and top edges are not equal, the offset will be suppressed and the φ_0 junction survives. In Figs. 8(a) and 8(b) we choose L_1 (L_2) as the junction length of top (bottom) edge, and calculate the ϕ-dependent J and G for different L_1 and L_2. Although the ferromagnetic exchange field is applied in the both edges, the φ_0 junction appears and is shown in Fig. 8(b) clearly. In the same way, from Eq. (20), if $\varepsilon = \pm\Delta(T)\cos(\frac{\phi}{2} + \frac{\lambda_{\mathrm{AF}}}{\hbar v'_{\mathrm{F}}}L_2) = \pm\Delta(T)\cos(\frac{\phi}{2} + 2p\pi - \frac{\lambda_{\mathrm{AF}}}{\hbar v'_{\mathrm{F}}}L_1)$ with p the integer, two opposite phases from the two edges offset each other absolutely. In other words, if $\lambda_{\mathrm{AF}}(L_1 + L_2) = 2p\pi/\hbar v'_{\mathrm{F}}$, the 0 and π junctions will appear in the presence of λ_{AF}. The phase-dependent Josephson current and free energy, shown in Figs. 8(c) and 8(d), confirm our analysis.

B. Modification of Fermi velocity in edge states

The previous researches on the π and φ_0 junctions are focused on the translational dispersion relation without modifying the Fermi velocity [2,3,12,13,15,18]. The research on the velocity-influenced Josephson junction has been lacking and here it seems an opportunity to fill this gap. We will show that the Fermi velocity of edge states can be modified by the off-resonant light, in the absence of exchange constants λ_{F} and λ_{AF}, and derive the ABS levels from Eq. (12) as

$$\varepsilon = \pm\Delta(T)\cos\left[\frac{\phi}{2} - \frac{(E_{\mathrm{F}} - slE_z)L}{2\hbar}\left(\frac{1}{v_{\mathrm{F}}^s} - \frac{1}{\bar{v}_{\mathrm{F}}^s}\right)\right]. \tag{25}$$

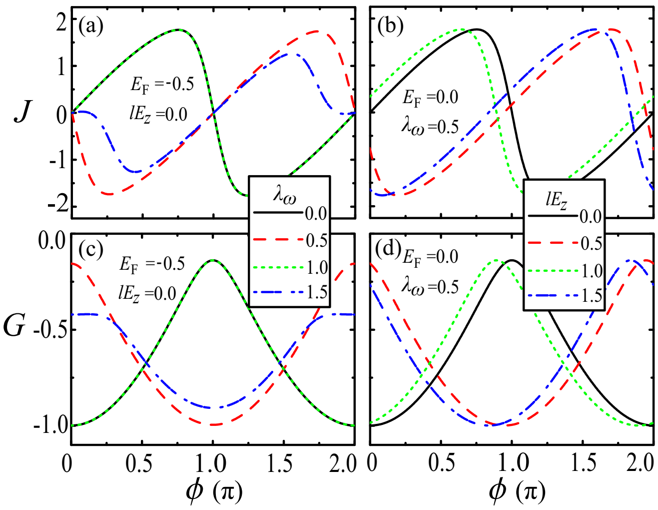

FIG. 9. Phase difference-dependent Josephson current [(a) and (b)] and free energy [(c) and (d)] are shown in different E_F, λ_ω, and lE_z. The junction length and the units for J and G are the same as the ones in Fig. 7.

It is found from this expression that a π (φ_0) junction can be generated by the interaction between the Fermi energy (electric field) E_F (lE_z) and illumination parameter λ_ω, as shown in Fig. 9. More importantly, the electric or light fields-modulated π and φ_0 junctions is feasible in experiment.

We should point out that the helicity of the edge states in silicene makes the edge state-supported Josephson current different from the bulk state-supported Josephson current. In fact, the position of Fermi energy is important for the Josephson current, especially in the presence of an antiferromagnetic exchange magnetization. If the Fermi energy is in the gap, then the edge states-induced φ_0 junction arises. When the Fermi energy is lifted and enters into the bulk states, the Josephson junction becomes a π junction. The switch between the φ_0 and π junctions can be realized by adjusting the Fermi energy.

V. EXPERIMENTAL MEASUREMENT

We consider that a silicene-based dc SQUID can be used to observe the π and φ_0 junctions here. The schematic diagram is shown in Fig. 10(a). The constraint condition between junctions 1 and 2 is [35]

$$(\varphi_a - \varphi_b) - (\varphi_c - \varphi_d) = 2\pi(\Phi/\Phi_0), \tag{26}$$

where $\Phi_0 = hc/2e$ is the fluxon. The total supercurrent through the ring is the sum of the supercurrents through the two junctions. If the critical currents are equal in both junctions, we obtain the total current

$$J_t = J_c[\sin(\varphi_a - \varphi_b + \varphi_1) + \sin(\varphi_c - \varphi_d + \varphi_2)], \tag{27}$$

where φ_1 and φ_2 represent the additional phases in junctions 1 and 2, respectively. Using the trigonometric formula, we get

$$J_t = 2J_c \cos(\pi\Phi/\Phi_0 + \varphi/2)\sin\gamma_0,\ \varphi = \varphi_1 - \varphi_2,$$
$$\gamma_0 = \tfrac{1}{2}(\varphi_a - \varphi_b + \varphi_1 + \varphi_c - \varphi_d + \varphi_2). \tag{28}$$

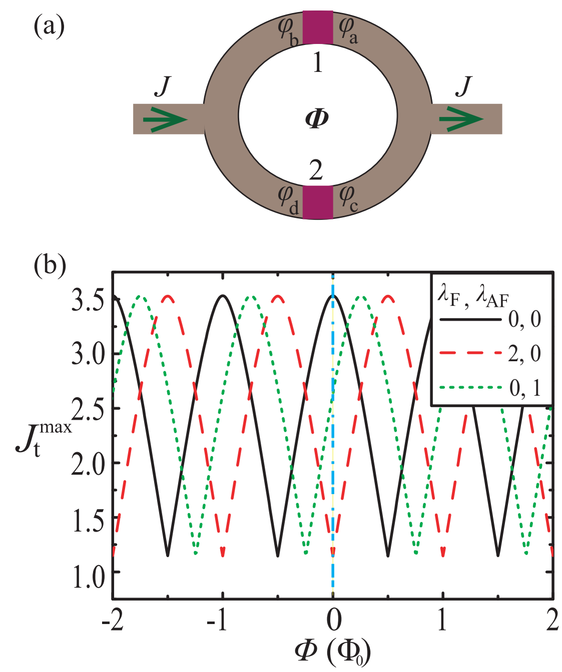

FIG. 10. (a) A schematic dc SQUID. (b) Magnetic flux-modulated maximal interference current supported by edge states in different parameters λ_F and λ_{AF}. The unit for J_t^{max} is the same as the one in Fig. 7.

It is no doubt that the maximal current through the dc SQUID is

$$J_t^{max} = 2J_c|\cos(\pi\Phi/\Phi_0 + \varphi/2)|. \tag{29}$$

From Eq. (29), if $\varphi = \varphi_1 - \varphi_2 = 0$, i.e., the two junctions are the same type, the π and φ_0 junctions cannot be distinguished. The best strategy is that the one junction is a π or φ_0 junction, the other is a 0 junction. However, the critical currents in different junctions seem to be not equal, which is required to calculate J_t^{max} numerically. In Fig. 10(b), one can find that the interference pattern of Josephson current in $0-\pi$ $(0-\varphi_0)$ SQUID is different from the one in 0-0 SQUID distinctly. Certainly it is easy to infer that the π junction arising from the bulk states and the φ_0 as well as π junction coming from the modified Fermi velocity have the same interference pattern as the one shown in Fig. 10(b). The theoretical calculations provide a reference for experiment.

VI. CONCLUSIONS

In summary, we have studied the Josephson effect in a silicene-based Josephson junction modulated by a perpendicular electric field, an antiferromagnetic exchange magnetization, a ferromagnetic exchange field, and an off-resonant light, applied in the middle region of the Josephson junction.

In the case of the bulk states, the valley polarization from the interaction between the antiferromagnetic exchange magnetization and spin-orbit coupling leads to a π junction, which is different from the case of spin polarization from the ferromagnetic exchange field.

In the case of the edge states, there are two different types of mechanism, the translational dispersion and the modified Fermi velocity are effective for realizing the π and φ_0 junctions. For the first mechanism, when a ferromagnetic exchange field is applied in both edges, a π junction is generated while an antiferromagnetic exchange magnetization induces a φ_0 junction. Interestingly, if the junction lengths of the bottom and top edges are not equal, junction length-dependent additional phases from two edges will lead to an anomalous phenomenon that the ferromagnetic exchange field (antiferromagnetic exchange magnetization) induces a φ_0 (π) junction. For the second mechanism, a π junction can be generated by the interaction between the Fermi energy and the off-resonant light. Meaningfully, a φ_0 junction can be manipulated simply by an electric field.

It is proposed that a silicene-based dc SQUID can be used to testify the π and φ_0 junctions. Our findings reveal the difference between the bulk states and topological edge states on the superconducting transport, and provide an alternative approach for realizing the π and φ_0 junctions.

ACKNOWLEDGMENTS

This work was supported by the State Key Program for Basic Research of China (Grant No. 2015CB921202) and the National Natural Science Foundation of China (Grants No. 11074108 and No. 11504179).

[1] J. Linder and T. Yokoyama, Phys. Rev. B **89**, 020504(R) (2014).
[2] X. Zhou and G. Jin, Phys. Rev. B **94**, 165436 (2016).
[3] A. Liebsch, Phys. Rev. B **84**, 180505(R) (2011).
[4] A. F. Andreev, Sov. Phys. JETP **19**, 1228 (1964).
[5] I. O. Kulik, Sov. Phys. JETP **30**, 944 (1970).
[6] B. D. Josephson, Rev. Mod. Phys. **46**, 251 (1974).
[7] A. I. Buzdin, L. N. Bulaevskii, and S. V. Panyukov, Pis'ma Zh. Eksp. Teor. Fiz. **35**, 147 (1982) [JETP Lett. **35**, 178 (1982)].
[8] V. V. Ryazanov, V. A. Oboznov, A. Yu. Rusanov, A. V. Veretennikov, A. A. Golubov, and J. Aarts, Phys. Rev. Lett. **86**, 2427 (2001).
[9] A. I. Buzdin, Rev. Mod. Phys. **77**, 935 (2005).
[10] A. Buzdin and A. E. Koshelev, Phys. Rev. B **67**, 220504(R) (2003).
[11] H. Sickinger, A. Lipman, M. Weides, R. G. Mints, H. Kohlstedt, D. Koelle, R. Kleiner, and E. Goldobin, Phys. Rev. Lett. **109**, 107002 (2012).
[12] A. Buzdin, Phys. Rev. Lett. **101**, 107005 (2008).
[13] T. Yokoyama, M. Eto, and Y. V. Nazarov, Phys. Rev. B **89**, 195407 (2014).
[14] G. Campagnano, P. Lucignano, D. Giuliano, and A. Tagliacozzo, J. Phys.: Condens. Matter **27**, 205301 (2015).
[15] K. N. Nesterov, M. Houzet, and J. S. Meyer, Phys. Rev. B **93**, 174502 (2016).
[16] A. Zazunov, R. Egger, T. Jonckheere, and T. Martin, Phys. Rev. Lett. **103**, 147004 (2009).
[17] D. B. Szombati, S. Nadj-Perge, D. Car, S. R. Plissard, E. P. A. M. Bakkers, and L. P. Kouwenhoven, Nat. Phys. **12**, 568 (2016).
[18] A. M. Black-Schaffer and J. Linder, Phys. Rev. B **83**, 220511(R) (2011).
[19] M. Ezawa, J. Phys. Soc. Jpn. **84**, 121003 (2015).
[20] M. Ezawa, Phys. Rev. Lett. **109**, 055502 (2012).
[21] M. Ezawa, Phys. Rev. Lett. **110**, 026603 (2013).
[22] M. Ezawa, Phys. Rev. Lett. **114**, 056403 (2015).
[23] X. Zhou, Y. Xu, and G. Jin, Phys. Rev. B **92**, 235436 (2015).
[24] Y. Xu, X. Zhou, and G. Jin, Appl. Phys. Lett. **108**, 203104 (2016).
[25] S.-I. Chu and D. A. Telnov, Phys. Rep. **390**, 1 (2004).
[26] X. Li, T. Cao, Q. Niu, J. Shi, and J. Feng, Proc. Natl. Acad. Sci. USA **110**, 3738 (2013).
[27] M. Ezawa and N. Nagaosa, Phys. Rev. B **88**, 121401(R) (2013).
[28] H.-J. Kwon, K. Sengupta, and V. M. Yakovenko, Eur. Phys. J. B **37**, 349 (2004).
[29] L. Fu and C. L. Kane, Phys. Rev. B **79**, 161408(R) (2009).
[30] D. M. Badiane, M. Houzet, and J. S. Meyer, Phys. Rev. Lett. **107**, 177002 (2011).
[31] E. A. Demler, G. B. Arnold, and M. R. Beasley, Phys. Rev. B **55**, 15174 (1997).
[32] Y. Matsuda and H. Shimahara, J. Phys. Soc. Jpn. **76**, 051005 (2007).
[33] P. Fulde and R. A. Ferrell, Phys. Rev. **135**, A550 (1964).
[34] A. I. Larkin and Yu. N. Ovchinnikov, Sov. Phys. JETP **20**, 762 (1965).
[35] M. Tinkham, *Introduction to Superconductivity*, 2nd ed. (McGraw-Hill, New York, 1996).
[36] V. A. Oboznov, V. V. Bol'ginov, A. K. Feofanov, V. V. Ryazanov, and A. I. Buzdin, Phys. Rev. Lett. **96**, 197003 (2006).
[37] G. Annunziata, H. Enoksen, J. Linder, M. Cuoco, C. Noce, and A. Sudbø, Phys. Rev. B **83**, 144520 (2011).